

Three-dimensionally interconnected multi-bus-line bidirectional optical backplane

Gicherl Kim

Ray T. Chen, FELLOW SPIE

University of Texas at Austin

Department of Electrical and Computer
Engineering

Microelectronic Research Center

J.J. Pickle Research Campus Building 160

10100 Burnet Road

Austin, Texas 78758

E-mail: gckim@mail.utexas.edu

Abstract. The concept of a three-dimensionally interconnected optical backplane for a high-performance system containing multichip module boards, operating at 850 nm, is introduced. The backplane reported here employs 2-D vertical-cavity surface-emitting lasers (VCSELs) and photodetector arrays as transceivers. By integrating 250- μm -pitch 2-D VCSELs, microlenses, and photodetector arrays into our backplane design, we have demonstrated a multi-bus-line optical backplane and experimentally realized this architecture with 2-D VCSEL and detector arrays while using the third dimension as the signal-propagating direction. Such an approach greatly increases the aggregate bandwidth of the backplane. Packaging issues such as misalignment, cross talk, and signal-to-noise ratio are studied. Eye diagrams up to 1.5 GHz were obtained with clear eyes, and the frequency response of a single bus line shows a bandwidth of 2.5 THz. © 1999 Society of Photo-Optical Instrumentation Engineers. [S0091-3286(99)00409-2]

Subject terms: optical backplane; holographic gratings; VCSEL arrays.

Paper 980474 received Dec. 28, 1998; revised manuscript received Mar. 22, 1999; accepted for publication Mar. 25, 1999.

1 Introduction

Optical interconnections have been of interest at all levels in digital computers for applications between mainframes, modules, boards, chips, and even points within a chip. Optics is ideally suited for implementing these interconnection networks because of its inherent high speed, high spatial bandwidth, low signal cross talk, and capability of wavelength-division (de)multiplexing through common media. Optical backplanes utilize optical signals to realize communications for board-to-board interconnection; each board is equipped with an optoelectronic converter (laser diode and photodetector) for the emission and detection of modulated optical signals. Optical interconnection provides the potential for a higher data rate for each bus channel and the advantage of reduced transmission-line-related problems.

In the past few years, several optical bus architectures based on the optical backplane concept have been proposed. These architectures include waveguide bus systems,¹ substrate-mode guided-wave bus systems implemented with waveguiding plates and holographic coupling elements,^{2,3} and free-space bus systems implemented through free-space optical interconnects.⁴

Although optoelectronics is increasingly attractive for backplane applications, difficulties associated with optoelectronic systems, such as misalignment and losses due to transition between optical and electrical signals, have limited the popularity of optics for interconnection. Other efforts in enhancing performance of the backplane are mainly devoted to increasing the bandwidth. The backplane bandwidth is defined as the product of the data-bus width and the data rate for each bus channel. Increasing the number of the bus lines can thus multiply the bus bandwidth.

There have been several different approaches^{5,6} to utilizing array devices. Among them, a number of recent attempts have been stimulated by advances in VCSEL technology. An attractive feature of VCSELs is their capability of being fabricated into uniform, individually addressable one- or two-dimensional arrays.^{7,8} Many optical interconnection systems taking advantage of these VCSEL arrays have been developed or manufactured.

In this paper, we report a three-dimensionally interconnected bidirectional optical backplane made by integrating VCSELs, lenses, doubly multiplexed holographic gratings, and photodetector arrays into our design. The characteristics of two-dimensional arrays for backplane interconnects are investigated. Packaging- and wavelength-instability-induced misalignments are studied, and graded index (GRIN) lenses or microlenses are introduced into our system, which greatly lessens the alignment difficulties. The power consumption of the system is considered also, and the ranges of allowable laser power input are specified. The bandwidth and data-transfer integrity of the device have been measured.

2 Multi-Bus-Line Optical Backplanes

Current efforts in enhancing the performance of backplanes are mainly devoted to increasing their aggregate bandwidth. Array devices should be useful in increasing the aggregate throughput of a backplane. Several approaches utilize array devices, among which the VCSEL as a transmitter array has evolved into an efficient and reliable device. By taking advantage of one- and two-dimensional VCSELs and photodetector arrays, and employing multiplexed holographic gratings, we propose and demonstrate a performance-enhanced optical backplane with multiple 1-D and 2-D bus lines.

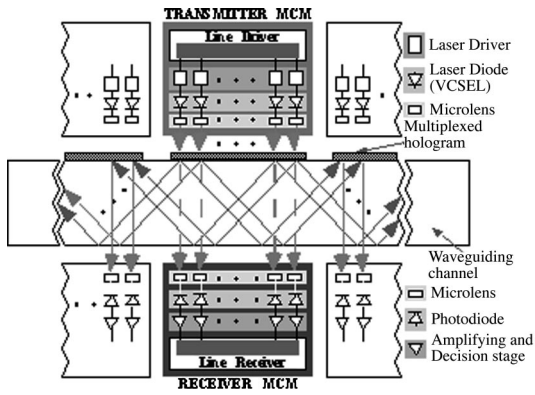


Fig. 1 Detailed diagram of waveguiding structure and transmitter and receiver modules of the proposed multi-bus-line backplane.

The previously demonstrated bidirectional optical backplane³ has only one bus line. By incorporating arrays of transmitter and receiver multichip modules on each side of the waveguiding channel, multi-bus-line backplane architecture can easily be implemented as shown in Fig. 1. In this design we utilize fanouts directed to the opposite side of the transmitters. This arrangement will result in a simpler transceiver design and ease the system packaging. Although we use the same waveguiding structure provided by the array of multiplexed holograms using DuPont photo-polymer film (HRF-600X001-20) and the waveguiding plate (refractive index 1.52), the overall design must be changed to integrate with electrical processor/memory boards. The center of one hologram is separated from those of the adjacent ones by 3 cm, which is the standard inter-board distance in the electrical backplane environment.

Figure 1 shows a detailed diagram of the multi-bus-line backplane using VCSEL and photodetector arrays, and also indicates the necessary components integrated into the transmitter and receiver multichip modules. As there is another set of fanouts directed to the transmitter modules, optical isolators are included on the transmitter modules to block them. Because the detector arrays just opposite to the transmitter arrays are on the same board, they do not need to communicate, and the corresponding beams are marked as dashed arrows. When the guided optical signals are packed closely with each other, cross talk between the adjacent channels may degrade the performance of the sys-

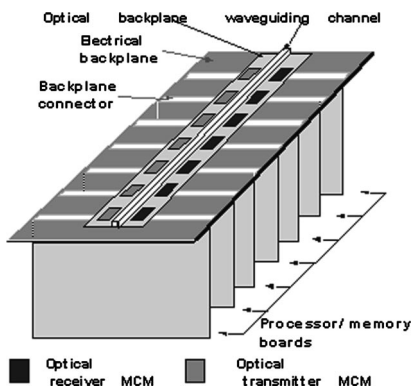


Fig. 2 Overall architecture of the proposed backplane.

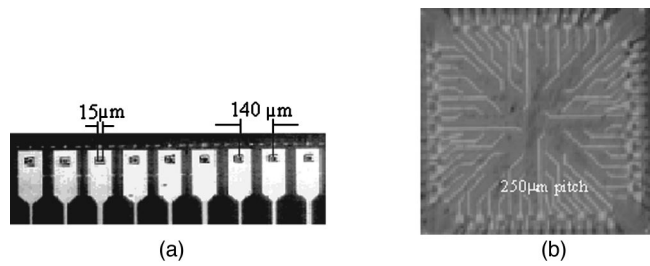


Fig. 3 VCSELs; (a) 1×32, 140-μm-pitch 1-D array, (b) 8×8, 250-μm-pitch 2-D array.

tem. The causes of this cross talk can be misalignment of the adjacent channels or spreading of the optical signal spots with propagation. Both of these lead to partial overlap among the optical signals from adjacent channels at the output ports.

The overall architecture employing the design of Fig. 1 is shown in Fig. 2. The arrangement of the transceivers on the backplane is in a plane perpendicular to the processor/memory boards. Another difference between this design and the previous one³ is that here the communication and conversion occur at the back of the backplane, while for the previous one they occur at the interface between the backplane and the boards.

Figure 3 shows the picture of the VCSEL arrays we currently use in our lab. The device has a total of 32 VCSELs for 1-D applications and 64 VCSELs (8×8) for 2-D applications, operating at a wavelength of 0.85 μm. The arrays have 140- and 250-μm pitch, respectively. The output power was measured at about 1 to 2 mW at 10-mA operating current. The experimental curves of current versus voltage and output power versus current at room temperature show a threshold voltage of ≈1.5 V and a threshold current of ≈4 mA. At a current of ≈37 mA, the output from the VCSEL reaches a maximum of ≈8.7 mW. After that, the output decreases with the increase of current. By measuring the full width at half maximum (FWHM) sizes of the two spots, the emission angle of the VCSEL turned out to be 5.7 deg.

Figure 4 shows experimental results on the proposed backplane with three bus lines (1-D). The separation between two lines is 140 μm, which corresponds to VCSELs 1 and 2 on the 1-D 32-VCSEL arrays of 140-μm pitch. A further improvement in the performance of the multi-bus-

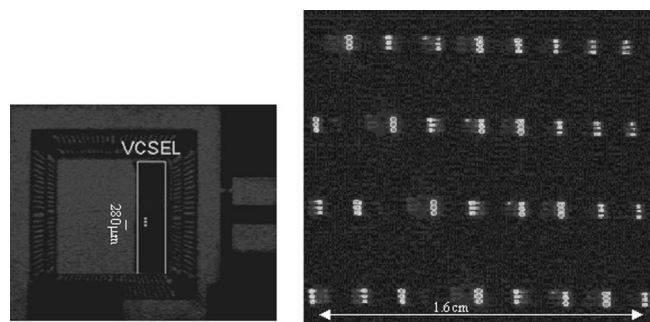


Fig. 4 Photograph of bidirectional optical backplane with 1-D bus lines: three bus lines with the 1st, 2nd, 3rd, and 4th channels functioning as the input couplers.

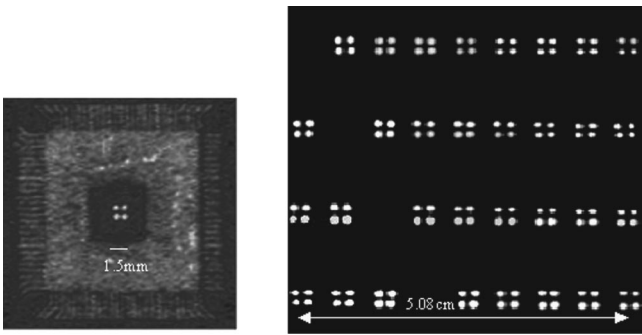


Fig. 5 Photograph of bidirectional optical backplane with 2-D matrix of bus lines (four for this case). The input/output configurations are the same as in Fig. 4.

line backplane can be achieved by using 2-D VCSELs and photodetector arrays instead of 1-D arrays, so that the real estate of the backplane can be effectively utilized. The results are shown in Fig. 5, where the input/output configurations of the backplane with four 2x2 bus lines are shown.

3 Alignment Consideration

Several factors affect the packaging of an optical interconnection device when integrated with source lasers and photodetectors. The most important ones are lateral misalignment, angular misalignment, wavelength instability, and divergence of spot size.

3.1 Lateral and Angular Misalignments

Lateral misalignment means the misalignment of the device position due to the inaccuracy in its *x* and *y* directions. Lateral misalignment can be divided into absolute and relative misalignment. With current self-aligned flip-chip solder-bump bonding process,⁹ the absolute lateral misalignment can be controlled with an accuracy of $\approx 1 \mu\text{m}$. Once coupled into the substrate, the signal beam travels towards the photodetector, and a lateral misalignment of the laser beam results in an equal spatial shift of the output signal beam.

The influence of angular misalignment on lateral misalignment arises from the phase mismatch between the input signal beam and the grating vector when the incident angle deviates from the Bragg angle. Figure 6 shows the phase-matching condition of a hologram for surface-normal coupling. For Bragg diffraction, we have¹⁰

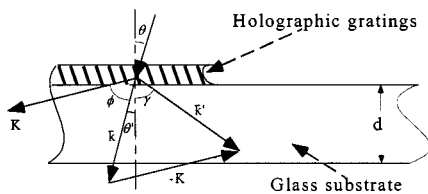


Fig. 6 Phase-matching diagram correlating the grating vector **K**, the incident beam **k**, and the diffracted beam **k'** for a slanted holographic grating element.

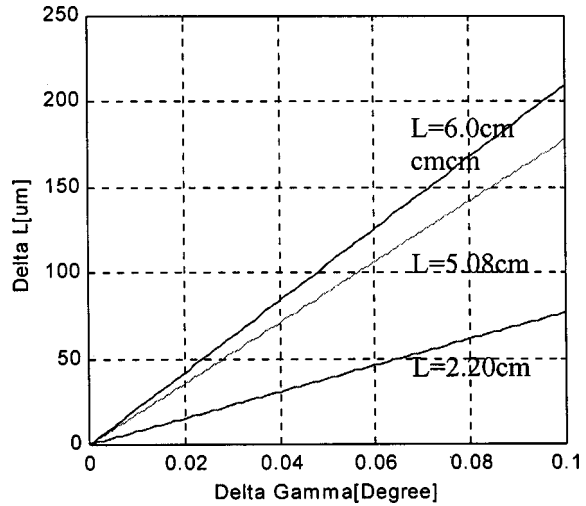


Fig. 7 Variation of spatial position of fanout beam on the device surface with respect to the angular misalignment of the input signal beam.

$$\begin{pmatrix} -\sin \gamma \\ \cos \gamma \end{pmatrix} = \begin{pmatrix} \frac{\sin \theta}{n} - \frac{K}{\beta} \sin \phi \\ \left(1 - \frac{\sin^2 \theta}{n^2} - \frac{K}{\beta} \cos \phi\right)^{1/2} \end{pmatrix}, \quad (1)$$

where *n* is the refractive index of the hologram, $\beta (= 2\pi n/\lambda)$ is the propagation constant of light with wavelength λ , and the meanings of γ , θ , and *K* are as shown in Fig. 6. After eliminating ϕ and differentiating the resulting equation, we have

$$\Delta \gamma = \frac{\left[\sin \theta - n \left(\frac{K^2}{2\beta^2} - 1 \right) \sin \gamma \right] \cos \theta}{\left[\left(\frac{K^2}{2\beta^2} - 1 \right) \sin \theta - n \sin \gamma \right] n \cos \gamma} \Delta \theta. \quad (2)$$

If the number of total internal reflections is *m* and thickness of the substrate is *t*, the corresponding device length is $L = mt \tan \gamma$. A variation of the angle of the input light beam leads to a spatial shift of the fanout beam on the device surface of

$$\Delta L = \frac{\tan(\gamma + \Delta \gamma) - \tan \gamma}{\tan \gamma} L. \quad (3)$$

This relation is schematically shown in Fig. 7 for the optical backplane with nine interconnected boards. In our calculation, we have assumed the wavelength of the source laser as $\lambda = 850 \text{ nm}$, and $n = 1.512$ (polymer waveguide), $\theta = 0 \text{ deg}$ (surface-normal), and $\gamma = 45 \text{ deg}$. We see from Fig. 7 that for small angular misalignment of the input light beam, ΔL changes linearly with $\Delta \theta$. However, Fig. 7 also shows that the control of the angular alignment is not an easy task. To keep the spatial shift of the output signal beam below an error range of $\pm 50 \mu\text{m}$ [for a silicon avalanche photodiode (APD), a typical size of the active area is on the order of $\sim 100 \mu\text{m}$ at 1 GHz], the angular

misalignment for 2.2-cm propagation should be within ± 0.065 deg. For an optical backplane device with substrate thickness of 0.125 in., the distance between the first and the last output channel is 5.08 cm, the requirement is more stringent, and the angular misalignment should be controlled within ± 0.028 deg. This stringent requirement is significantly relaxed by applying a graded index (GRIN) lens or microlens.

3.2 Wavelength Instability

Variation of the lasing wavelength from the design value influences the spatial shift of the output signal beam via the same mechanism as does angular misalignment. In fact, this mechanism has been used in the design of a wavelength division demultiplexing (WDDM) device.¹³ The theory behind this mechanism is that a deviation in wavelength of the input signal beam will lead to an angular deviation of the diffracted beam from the Bragg angle. This produces a spatial shift of the output beam. The variation of the spatial position of a fanout beam on the device surface is linearly dependent on the wavelength shift of the signal beam. Generally, the emission linewidth from a VCSEL can be less than 1 Å.¹⁴ The misalignment due to this spectral width factor can thus be ignored, considering that the normal size of the photodetector active area is on the order of 100 μm. For a VCSEL with a three-quantum-well (QW) InGaAs/GaAs active region, the lasing wavelength varies with temperature at a rate of ≈ 0.5 Å/K.¹⁴ To maintain the spatial shift within ± 50 μm, the allowable temperature variation is ± 5.8 K, which is within the limits of contemporary optoelectronic temperature stability control.

For the VCSELs we employed, the active light-emitting window has a diameter of 5 μm and a lasing divergence angle of 5 deg. After propagating 2.2 cm in the substrate, the spot size becomes 615 μm. This enlargement of the spot size renders the photodetector incapable of responding in view of the ≈ 100 -μm size of the detector active region for a 1-Gbit/s system.^{11,12} To make the system practical, precise beam profile manipulation is required. Here we introduce GRIN lenses into our system. A 0.25-pitch GRIN lens is suitable for our application. After the signal beam from the VCSEL has traveled through the GRIN lens, it will be collimated. Theoretically, as long as the collimated beam remains incident surface-normally on the GRIN lens at the output end, it will be focused into a diffraction-limited spot. If the input signal beam has a misalignment $\Delta\theta$ in its input angle, then the ray matrix gives the spot shift at the focusing end as $\Delta r = \Delta\theta/N_0\sqrt{A}$, where N_0 is the refractive index on the central axis of the GRIN lens, and \sqrt{A} is the index gradient constant. At $\lambda = 0.85$ μm, $N_0 = 1.6457$, and $\sqrt{A} = 0.423$, with a misalignment angle of 2 deg, the shift of the output spot from the central axis of the GRIN lens is $\Delta r \approx 50$ μm, while without the GRIN lens, this same angular misalignment would give ≈ 1 mm from Eq. (3).

4 Power Requirement of an Optical Backplane

The required laser power for an optical interconnection device is determined by the efficiency of the input and output couplers and the receiver sensitivity. For our device, $P_{\text{out}} = \eta(1 - R)P_{\text{in}}$, where R is the reflectivity of input grating

coupler and η is the efficiency. Here R is around 11% without any antireflection coating, and from our previous report,⁵ the minimum output efficiency for a nine-board optimized backplane is 1.57%. With the sensitivity of 0.04 μW and dynamic range of 30 dB for APD receivers at 1 Gbit/s, the minimum power input is 3.0 μW ($= 0.04/[0.0157 \times (1 - 0.11)]$), and the maximum power of a signal that can be received by a receiver without distortion is 40 μW [$= 0.04 \mu\text{W} \times 10^3$ from $10 \log(P_{\text{max}}/0.04 \mu\text{W}) = 30$ dB]. Since the required maximum output efficiency of our optimized backplane is 74.5%, the maximum required laser power input is 60 μW ($= 40 \mu\text{W}/[0.745 \times (1 - 0.11)]$). Thus, the allowable range of the input laser power for our optimized optical backplane is 3.0 to 60 μW, which can be easily achieved using state-of-the-art VCSEL technology.

5 Measurement of Data-Transfer Integrity

Except for the power requirement, the performance of an optical interconnection device is characterized by its bandwidth and data-transmission integrity. In this section, we demonstrate the experimental performance of our devices in these respects.

5.1 System Bandwidth and Signal Response Measurements

One of the advantages of optical interconnects over traditional electrical circuits is the much wider bandwidth of optics. The bandwidth, which determines the highest speed the information can be transferred without distortion, was measured in our experiment by the frequency response of the device. In our experimental setup, a laser beam of 4.3 W at a wavelength of 514.6 nm from an argon laser (Coherent I-90 Plus) is used to pump a Clark-MXR Ti:sapphire mode-locked laser, whose output is then fed into the optical interconnection device. A Clark-MXR auto correlator (AC-150) analyzes the output signal from the device and sends the results to an ODL data acquisition system. The output measurement from the mode-locked laser showed that the demonstrated pulse has a speed of 150 fs with a power of 0.4 W centered at 850 nm. After correlation, the profiles of the pulse signal with and without the interconnection device can be obtained. The propagation distance of the pulse inside the device is 5.08 cm, which is equivalent to propagation from the first to the ninth channel of our optical backplane device. Due to the dispersion of the backplane material, the pulse from the backplane experiences broadening relative to the reference pulse.

By making a fast Fourier transform (FFT) of the output pulse from time domain to frequency domain, the frequency response of the optical interconnection device can be automatically determined when compared with the FFT result of the reference pulse, which is directly coupled into the correlator from free space. Figure 8 shows the FFT results for the reference and the device output pulses. It is clear from Fig. 8 that a 2.5-THz (2500-GHz) bandwidth is expected from the optical interconnection system.

5.2 Eye-Diagram Measurements

By overlaying sweeps of different segments of a long data stream driven by a master clock, we can get an eye diagram

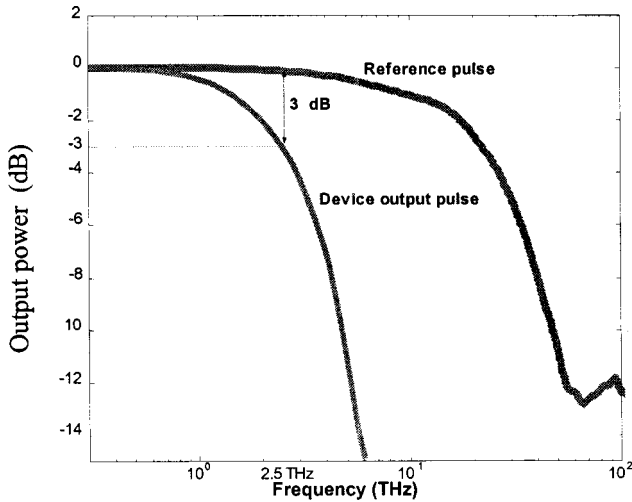


Fig. 8 FFT results for the reference and device output pulses.

on the screen of a storage oscilloscope (analog or digital). In communication industries, the eye diagram is used to observe and analyze the performance of circuits that drive the transfer of digital data streams. Ideally, when many traces of randomly generated data series have been overlaid, positive- and negative-going pulses are superimposed on each other, and a pattern like a rectangular box results. In practice, especially when the displayed signal has traversed an imperfect communications channel, the traces do not lie perfectly atop one another, and a classic eye pattern results.

In order to measure the eye diagrams of our optical interconnection devices, the random bit pattern from a 3-GHz pulse generator (HP8133A) is used to current-modulate an 822-nm semiconductor laser transmitter (FOT-FP-820-1M/3G-5/125-0 from Lawrence Labs, Ltd.). After being collimated and passing through the device, the optical signal from the transmitter is focused onto a high-speed (1.5-GHz) *pin* silicon photodiode (Hamamatsu S4753). The output of the receiver is then analyzed by a digitizing oscilloscope (HP54120A).

To demonstrate the performance of our device, eye diagrams at speeds of 500 MHz, 1 GHz, and 1.5 GHz were measured with and without the device for comparison. The final experimental results with the 1.5-GHz signal are shown in Figs. 9 and 10. Much information can be gained from the measurement of the eye diagram. The horizontal

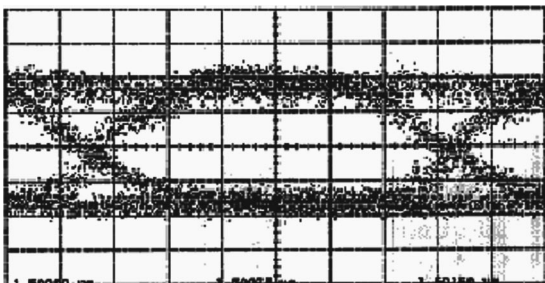


Fig. 9 Eye diagram of the system output as a function of data rate without the interconnection device at 1.5 GHz.

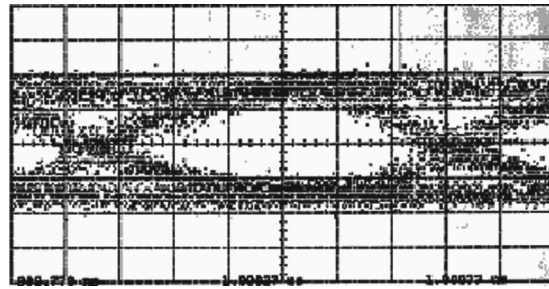


Fig. 10 Eye diagram of the system output as a function of data rate with the interconnection device at 1.5 GHz.

dark areas of the display show the time-voltage combinations at which the signal spends most of its time, while the fainter crosslike areas correspond to less frequent (but possibly more troublesome) events. The clear inside portion of the display is known as the eye. A very clean signal will have a large, clear eye, while a noisy, low-quality signal will have a smaller one. The eye can become completely closed if the data signal has a lot of timing jitter with respect to the master clock, if the pulse widths are incorrect, or if varying amounts of noise and attenuation cause the signal amplitude to vary excessively. By comparing the eye diagrams before (Fig. 9) and after (Fig. 10) the insertion of our optical interconnection device, we see that the signal noise is mainly from the test system, and the device contributes no noticeable distortion to the signal. Even up to data speeds as high as 1.5 GHz, our experiment shows very clear, open eyes, both with and without the device. For speeds higher than 1.5 GHz, the experiments were limited by the 1.5-GHz bandwidth of the receiver.

5.3 Crosstalk Analysis and Signal-to-Noise Ratio

Currently, the commercially available GRIN lenses have a minimum radius of 0.5 mm. So in our experiment the minimum separation of the bus lines should be 1 mm. But due to the cross talk between the adjacent bus lines, this minimum separation must be determined according to the requirement of the signal-to-noise ratio (*S/N*). Even with a collimating GRIN lens, because of the alignment error and the Gaussian beam effect, the cross talk still needs to be studied.

If there are two adjacent receivers with radius *R* and at a distance *d* in a polar coordinate system, we obtain the total noise collected by detector as

$$P_{\text{noise}} = 2 \int_{d-R}^{d+R} \int_{-\arccos[(\rho^2+d^2-R^2)/2\rho d]}^{\arccos[(\rho^2+d^2-R^2)/2\rho d]} P \cdot \rho \, d\theta \, d\rho, \quad (4)$$

where ρ and θ are the polar radius and angle, respectively. The factor 2 in Eq. (4) is due to the noise from the laser beam located at distance $2d$. By inserting the Gaussian intensity distribution into Eq. (4), we have

$$P_{\text{noise}} = 4P_0 \int_{d-R}^{d+R} \exp\left(-2 \frac{\rho^2}{w^2}\right) \arccos \frac{\rho^2 + d^2 - R^2}{2\rho d} \, d\rho. \quad (5)$$

The signal intensity collected by each detector is

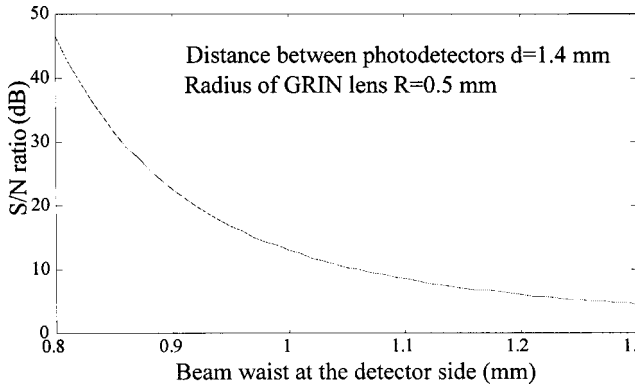


Fig. 11 Variation of S/N with the beam waist (with $R=0.5$ mm) for the backplane with 1-D arrays of VCSELs and detectors.

$$P_{\text{signal}} = \int_0^R P \cdot 2\pi\rho \, d\rho = \frac{\pi w^2}{2} P_0 \left[1 - \exp\left(-2\frac{R^2}{w^2}\right) \right]. \quad (6)$$

With the above equations, we can calculate S/N . The variations of S/N with the lens radius and beam waist were calculated numerically. The result is shown in Fig. 11 with a detector separation of 1.4 mm and a lens radius of 0.5 mm. From this figure we see that for our experiment, in which the radius of the lens is 0.5 mm, cross talk is negligible until the beam waist reaches 1 mm, at which $S/N \approx 15$. Because of the alignment error of the collimating lens, the laser beam coming out of the lens is divergent. We see that for our backplane with a total length of 5.08 cm, the spreading of the laser beam is around 0.8 mm due to the beam divergence. So the S/N of our device is greater than 15. A similar calculation gives the relationship between the beam waist and the divergence angle for a propagation distance of 5.08 cm. We see from this that, if S/N is to be greater than 15 (i.e., $w \leq 1$ mm), the divergence angle can be as large as 1 deg.

For the backplane with 2-D VCSEL and photodetector arrays, if only cross talk from the nearest lasers is considered, the noise power can easily be obtained as

$$P_{\text{noise}} = 8P_0 \left(\int_{d-R}^{d+R} \exp\left(-2\frac{\rho^2}{w^2}\right) \arccos \frac{\rho^2 + d^2 - R^2}{2\rho d} \, d\rho + \int_{\sqrt{2}d-R}^{\sqrt{2}d+R} \exp\left(-2\frac{\rho'^2}{w^2}\right) \times \arccos \frac{\rho'^2 + 2d^2 - R^2}{2\sqrt{2}\rho' d} \, d\rho' \right). \quad (7)$$

A plot of S/N versus beam waist (with $R=0.5$ mm) is shown in Fig. 12. From this figure, we see that for $R=0.5$ mm and $d=1.4$ mm, S/N is 15 when $w \approx 0.85$ mm. Also this shows that with the same values of d , R , and w , S/N is about half what it is with 1-D arrays of VCSELs and photodetectors. So the cross talk from the VCSELs in the diagonal directions can be concluded to be unimportant. This justifies our considering the cross talk only from the nearest VCSELs.

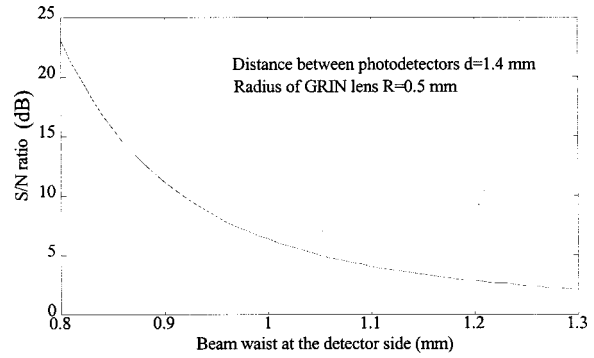


Fig. 12 Variation of S/N with the beam waist (with $R=0.5$ mm) for the backplane with 2-D arrays of VCSELs and detectors.

For 2-D applications, 8×8 VCSEL arrays with $250\text{-}\mu\text{m}$ pitch are commercially available. But the beam propagation performance depends on the emitting spot radius of the VCSEL and the focal length of the lens array. Therefore, the possible choice of focal length of the microlens is from 1.0 to 2.0 mm, and the lens pitch should be over $500 \mu\text{m}$ when the total propagation distance for nine boards is 5.08 cm. In the case of the 24-cm propagation distance (3.0-cm separation between boards), the focal length of lens must be 5.0 mm and the lens pitch more than $750 \mu\text{m}$. So another problem arises in the choice of microlens. We have a choice of lens pitch, but large-focal-length microlenses are difficult to make and time-consuming to fabricate.

6 Summary

We have characterized our bidirectional optical backplane for multiboard interconnects from the point of view of alignment, power requirement, and data transfer integrity. Both angular- and wavelength-instability-induced misalignment were discussed. By using a collimating lens in our design, we showed that the alignment constraint could be greatly relaxed. From the performance-optimized output results, we calculated the allowable laser input power range for the optical backplane, which is 3.0 to $60 \mu\text{W}$. The frequency response of our devices showed a bandwidth of 2.5 THz, which is very high. Eye diagrams up to 1.5 GHz have been demonstrated with clear eyes.

Finally, we further proposed and demonstrated a performance-enhanced bidirectional optical backplane, which is a three-dimensionally interconnected device with multiple bus lines. By employing VCSEL and photodetector arrays, we produced backplanes with 1-D and 2-D bus lines, having greatly increased bus bandwidth. The minimum pitch of a VCSEL array, which is the pitch for acceptable output crosstalk, is strongly dependent on the total propagation distance and focal length of lens; the minimum pitch for 5.08-cm propagation was $500 \mu\text{m}$ with focal length of 1 to 2 mm. It should be noted that further improvement of the throughput could be achieved by choosing proper system parameters within the same design concept.

Acknowledgment

This research is sponsored by DARPA, ONR, AFOSR, BMDO, Army Space and Missile Defense Command, 3M

Foundation, Cray research, and the ATP program of the state of Texas. The authors would like to thank the members of the JOP program from OIDA for providing the 2-D VCSEL, driver, and detector array.

References

1. L. W. Shacklette, K. M. T. Stengel, L. Eldada, C. Xu, and J. T. Yardley, "Polymeric waveguides for optical backplanes," *Proc. SPIE* **2467**, 107 (1995).
2. C. Sebillotte, "Holographic optical backplane for boards interconnection," in *International Conference on Advances in Interconnection and Packaging, Proc. SPIE* **1389**, 600 (1990).
3. S. Natarajan, C. Zhao, and R. T. Chen, "Bi-directional optical backplane bus for general purpose multi-processor board-to-board optoelectronic interconnects," *J. Lightwave Technol.* **13**, 1031 (1995).
4. T. Sakano, T. Matsumoto, and K. Noguchi, "Three dimensional board-to-board free space optical interconnections and their application to the prototype multiprocessor: COSINE-III," *Appl. Opt.* **34**, 1815 (1995).
5. A. Takai, T. Kato, S. Yamashita, S. Hanatani, Y. Motegi, K. Ito, H. Abe, and H. Koderu, "200-Mb/s/ch 100-m optical subsystem interconnections using 8 channel 1.3-mm laser diode arrays and single-mode fiber arrays," *J. Lightwave Technol.* **12**, 260 (1994).
6. T. Nagahori, M. Itoh, I. Watanabe, J. Hayashi, and H. Honmou, "150Mbit/s/ch 12-channel optical parallel interface using an LED and a PD array," *Opt. Quantum Electron.* **24**, S479 (1992).
7. D. Vakhshoori, J. D. Wynn, and G. J. Zydzik, "8x18 top emitting independently addressable surface emitting laser arrays with uniform threshold current and low threshold voltage," *Appl. Phys. Lett.* **62**, 1718 (1993).
8. A. Von Lehmen, C. Chang-Hasnain, J. Wullert, L. Carrion, N. Stoffel, L. Florez, and J. Harbison, "Independently addressable InGaAs/GaAs vertical cavity surface emitting laser arrays," *Electron. Lett.* **27**, 583 (1991).
9. M. J. Wale and C. Edge, "Self-aligned flip-chip assembly of photonic devices with electrical and optical connections," *IEEE Trans. Compon., Hybrids, Manuf. Technol.* **13**, 780 (1990).
10. H. Kogelnik, "Coupled wave theory for thick hologram gratings," *Bell Syst. Tech. J.* **48**, 2909 (1969).
11. T. V. Muoi, "Optical design for high-speed optical-fiber system," *J. Lightwave Technol.* **LT-2**, 2430 (1983).
12. J. Wieland, H. Melchior, M. Q. Kearley, C. R. Morris, A. M. Moseley, M. J. Goodwin, and R. C. Goodfellow, "Optical receiver array in silicon bipolar technology with self-aligned, low parasitic III/V detectors for DC-1 Gbits/s parallel links," *Electron. Lett.* **27**, 2211 (1991).
13. M. M. Li and Ray T. Chen, "Two-channel surface-normal wavelength division demultiplexer using substrate guided waves in conjunction with multiplexed waveguide holograms," *Appl. Phys. Lett.* **66**, 262 (1995).
14. H. Deng, C. C. Lin, D. L. Huffaker, Q. Deng, and D. G. Deppe, "Temperature dependence of the traverse lasing mode in vertical-cavity lasers," *J. Appl. Phys.* **77**, 2279 (1995).

are in the area of optical interconnect devices such as WDM devices and fabrication techniques for holographic optical elements. His current research projects deal with optical backplanes for multiboard interconnects.



Ray T. Chen received the BS in physics in 1980 from the National Tsing Hua University, China, the MS in physics in 1983 from the University of California, San Diego, and a PhD in electrical engineering in 1988 from the University of California, Irvine. He joined the Department of Electrical and Computer Engineering at The University of Texas at Austin in 1992 and is currently an associate professor. Prior to that he was a director of the Electro-Optic Engineering

Department at the Physical Optics Corporation. Dr. Chen's research group has been working on over 50 awarded research programs sponsored by many subdivisions of DOD, NSF, DOE, NASA, the state of Texas, and private industries such as Cray Research, GE, Honeywell, 3M, Boeing, Physical Optics Corporation, MCC, and Novex Corporation. The research topics cover guided wave and free-space optical interconnects, polymer-based integrated optics, polymer waveguide amplifier, graded index polymer waveguide lenses, active optical back planes, traveling wave electro-optic polymer waveguide modulators, optical control of phased array antenna, GaAs all optical cross bar switch, holographic lithography, and holographic optical elements. Dr. Chen has served as the chairman and program committee member for over 25 domestic and international conferences organized by SPIE, OSA, IEEE, and PSC. He is also an invited lecturer for the short course on optical interconnects for the international technical meetings organized by SPIE. The optical interconnects research group at UT Austin has published over 230 research papers including 35 invited papers. Dr. Chen has served as a consultant for various federal government agencies and private companies and delivered numerous invited talks in the professional societies. Dr. Chen is a member of IEEE, LEOS, SPIE, OSA, and PSC, and holder of the Temple Foundation Endowed Faculty Fellowship No. 4.



Gicherl Kim received his BS and MS degrees in physics from Inha University, Korea, in 1989 and 1991, respectively. From 1991 to 1997, he was a researcher at the Agency for Defense Development (ADD), where he performed researches in computational electromagnetics (FEM and BEM), design and fabrication of magnetic sensors, and optimization techniques for target detection and degaussing. He is presently a PhD student in electrical and computer engineering at University of Texas at Austin. His research interests